Wave-induced velocities inside a model seagrass bed

Wave-induced velocities inside a model seagrass bed

Mitul Luhar,[1] Sylvain Coutu,[2] Eduardo Infantes,[3] Samantha Fox,[1] and Heidi Nepf[1]

Received 15 April 2010; revised 8 July 2010; accepted 13 August 2010; published 2 December 2010.

[1] Laboratory measurements reveal the flow structure within and above a model seagrass meadow (dynamically similar to *Zostera marina*) forced by progressive waves. Despite being driven by purely oscillatory flow, a mean current in the direction of wave propagation is generated within the meadow. This mean current is forced by a nonzero wave stress, similar to the streaming observed in wave boundary layers. The measured mean current is roughly four times that predicted by laminar boundary layer theory, with magnitudes as high as 38% of the near-bed orbital velocity. A simple theoretical model is developed to predict the magnitude of this mean current based on the energy dissipated within the meadow. Unlike unidirectional flow, which can be significantly damped within a meadow, the in-canopy orbital velocity is not significantly damped. Consistent with previous studies, the reduction of in-canopy velocity is a function of the ratio of orbital excursion and blade spacing.

Citation: Luhar, M., S. Coutu, E. Infantes, S. Fox, and H. Nepf (2010), Wave-induced velocities inside a model seagrass bed, *J. Geophys. Res.*, *115*, C12005, doi:10.1029/2010JC006345.

1. Introduction

[2] Seagrasses, which occupy 10% of shallow coastal areas [*Green and Short*, 2003], are essential primary producers, forming the foundation for many food webs. Seagrass beds also damp waves, stabilize the seabed, shelter economically important fish and shellfish, and enhance local water quality by filtering nutrients from the water. On the basis of nutrient cycling services alone, the global economic value of seagrass beds was estimated to be 3.8 trillion dollars per year by *Costanza et al.* [1997]. Furthermore, numerous studies note higher infaunal density within seagrass beds [e.g., *Santos and Simon*, 1974; *Stoner*, 1980; *Irlandi and Peterson*, 1991]. *Peterson et al.* [1984] found that clams in seagrass beds had higher growth rates and also that the density of the bivalve, *Mercenaria mercaneria*, was five time greater in seagrass meadows than on adjacent sand beds. By damping near-bed water velocities, seagrasses reduce local resuspension and promote the retention of sediment [e.g., *Fonseca and Cahalan*, 1992; *Gacia et al.*, 1999; *Granata et al.*, 2001], thereby stabilizing the seabed. Reduced resuspension improves water clarity, leading to greater light penetration and increased productivity [*Ward et al.*, 1984]. Seagrasses are also a source of drag. Hence, waves propagating over seagrass beds lose energy [*Fonseca and Cahalan*, 1992; *Chen et al.*, 2007; *Bradley and Houser*, 2009].

[3] Some of the ecosystem services mentioned above (stabilizing the seabed, wave decay, shelter for fish and shellfish) arise because seagrasses are able to alter the local flow conditions. The nutrient cycling capability of seagrasses is limited both by the rate of water renewal within the bed and the rate at which the seagrasses are able to extract nutrients from the surrounding water, which, under some conditions, is limited by the diffusive boundary layer on the blades. Clearly, the hydrodynamic condition plays a major role in determining both the health of seagrass beds and their ecologic contribution. Previous studies have successfully described the flow structure for submerged vegetation subjected to unidirectional flow (currents) using rigid and flexible vegetation models [e.g., *Finnigan*, 2000; *Nepf and Vivoni*, 2000; *Ghisalberti and Nepf*, 2002, 2004, 2006]. A summary of unidirectional flow over submerged canopies can be found in the study by *Luhar et al.* [2008].

[4] For the case of oscillatory flow (waves), previous work has focused primarily on quantifying wave decay [e.g., *Fonseca and Cahalan*, 1992; *Kobayashi et al.*, 1993; *Méndez et al.*, 1999; *Mendez and Losada*, 2004; *Bradley and Houser*, 2009]. Other studies involving oscillatory flow include those by *Thomas and Cornelisen* [2003], who showed that nutrient uptake in seagrass beds was higher for wave conditions, and *Koch and Gust* [1999], who suggested that the periodic motion of seagrass blades could lead to enhanced mass transfer between the meadow and the overlying water column. Despite these insights, researchers have only recently begun to study the detailed hydrodynamics of submerged vegetation subjected to wave-driven oscillatory flow. *Lowe et al.* [2005a] studied the flow structure within a model canopy comprising rigid vertical cylinders and developed an analytical model to predict the magnitude of in-canopy velocity in the presence of waves. They used a simple friction coefficient to characterize the shear stress at the top of the

[1]Department of Civil and Environmental Engineering, Massachusetts Institute of Technology, Cambridge, Massachusetts, USA.
[2]Institut d'Ingénieurie de l'Environnement, Ecole Polytechnique Fédérale de Lausanne, Lausanne, Switzerland.
[3]Instituto Mediterráneo de Estudios Avanzados, IMEDEA (CSIC-UIB), Esporles, Spain.

0148-0227/10/2010JC006345

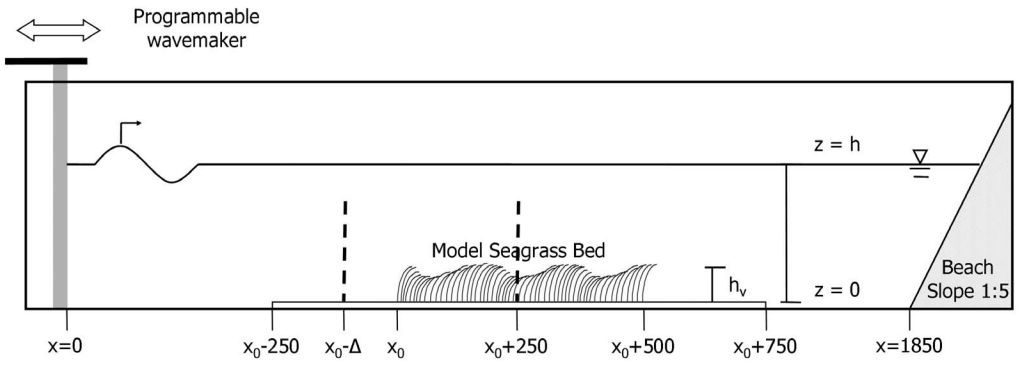

Figure 1. Schematic of experimental setup. The bold dashed line indicates measurement locations for the vertical profile. Not to scale.

canopy and drag and inertia coefficients to parameterize the hydrodynamic impact of the canopy elements.

[5] The present laboratory study investigates the flow structure within a model seagrass bed subject to propagating waves. The model is constructed with flexible blades that are dynamically similar to real seagrass blades [see *Ghisalberti and Nepf*, 2002]. Our experiments reveal that a unidirectional current is generated within the model seagrass bed when it is forced by purely oscillatory, wave-driven flow. This is, in some ways, analogous to viscous [*Longuet-Higgins*, 1953] and turbulent [*e.g.*, *Longuet-Higgins*, 1958; *Johns*, 1970; *Trowbridge and Madsen*, 1984; *Davies and Villaret*, 1998, 1999; *Marin*, 2004] streaming observed in wave boundary layers. The induced current could speed up the rate of water renewal within a meadow, enhancing the nutrient cycling capabilities of the seagrass. A directional bias in the dispersal of seeds and pollen could affect seagrass meadow structure. The induced current also has the potential to influence the net transport of sediment. Finally, the hydrodynamic drag exerted by the model vegetation leads to a reduction of in-canopy orbital velocities. We observed that the ratio of in-canopy to over-canopy velocity is significantly higher when the flow is oscillatory (tested here) compared to the unidirectional case tested by *Ghisalberti and Nepf* [2006]. This is in agreement with *Lowe et al.* [2005a]. As noted by *Lowe et al.* [2005b], larger in-canopy velocities could explain the higher nutrient uptake observed under oscillatory flows [*Thomas and Cornelisen*, 2003].

2. Theory

2.1. Linear Wave Theory and Boundary Layer Streaming

[6] In the absence of a canopy, linear wave theory [e.g., *Mei et al.*, 2005] leads to the following solutions for the horizontal (U_w) and vertical (W_w) oscillatory velocity fields for waves propagating over a flat bed,

$$U_w = a\omega \frac{\cosh kz}{\sinh kh}\cos(kx - \omega t), \tag{1a}$$

$$W_w = a\omega \frac{\sinh kz}{\sinh kh}\sin(kx - \omega t), \tag{1b}$$

and wave-induced dynamic pressure (p_w),

$$p_w = \rho \frac{\omega}{k} U_w = \rho g a \frac{\cosh kz}{\cosh kh}\cos(kx - \omega t). \tag{2}$$

In the equations above, ρ is the fluid density, g is the gravitational acceleration, a is the wave amplitude, ω is the wave radian frequency, k is the wave number, h is the water depth, x and z are the horizontal and vertical coordinates (z = 0 at the bed), and t is time. The water depth h refers to the distance from the bed to the mean water level (Figure 1). The frequency, wave number, and water depth are related by the dispersion relation, $\omega^2 = (kg)\tanh(kh)$. Throughout this paper, the subscript w refers to purely oscillatory flows (i.e., time average of zero). When we refer specifically to unidirectional flows (currents), the subscript c is used. Turbulent, fluctuating velocities are represented by lowercase letters with prime symbols (u', w').

[7] In addition to neglecting the nonlinear terms in the Navier-Stokes equations, linear wave theory assumes perfectly inviscid, irrotational motion. Under these assumptions, the horizontal and vertical velocities are exactly 90° out of phase with each other, as evidenced by equations (1a) and (1b). However, this solution does not satisfy the no-slip boundary condition at the bed. While the inviscid assumption is valid for most of the water column, viscosity is important in the bottom boundary layer, which for laminar flows is of thickness $O[(\nu/\omega)^{1/2}]$. Here, ν is the kinematic viscosity of water. The horizontal oscillatory velocity decays from the inviscid value (1a) at the outer edge of the boundary layer to zero at the bed because of viscosity. This modification to the inviscid solution causes a phase shift in the oscillatory velocities. The horizontal and vertical velocities are no longer exactly 90° out of phase, creating a steady, nonzero wave stress, $\langle U_w W_w \rangle \neq 0$ ($\langle\cdot\rangle$ denotes a time average). This wave stress is analogous to turbulent Reynolds stress. It represents a time-invariant momentum transfer out of the oscillatory flow and generates a mean current in the boundary layer. For laminar flows, the magnitude of this current, U_c, at the outer edge of the boundary layer is [*Longuet-Higgins*, 1953]

$$U_c = \frac{3}{4}(ka)\frac{a\omega}{\sinh^2 kh}. \tag{3}$$

The forces exerted by our model seagrass canopy also lead to a phase shift between the oscillatory velocities, resulting in a nonzero wave stress. Below, we present an overview of the forces exerted by the canopy on the wave flow [based on *Lowe et al.*, 2005a] followed by a new analysis estimating the mean flow generated within the canopy.

2.2. Canopy Forces

[8] *Lowe et al.* [2005a] described the water motion within a rigid canopy (a model coral reef) relative to the undisturbed flow above the canopy. Here, we consider the application of their model to a flexible model canopy (a model seagrass meadow). The geometry of the canopy is described by two dimensionless parameters, the frontal area per bed area, $\lambda_f = a_v h_v$, and the planar area per bed area, λ_p. Here, a_v is the frontal area per unit volume, and h_v is the vegetation height. Because of the forces exerted by the vegetation, the velocity scale within the meadow, $\hat{U}_m$, is reduced relative to that above the meadow, U_∞. The velocity scale inside the canopy, $\hat{U}_m$, represents a vertical average over the canopy height (denoted by the over-hat symbol).

[9] The velocity ratio, $\alpha = \hat{U}_m/U_\infty$, depends on the relative importance of the shear stress at the top of the meadow (ρu_{*hv}^2), the drag force exerted by the meadow ($(1/2)\rho C_D a_v |\hat{U}_m| \hat{U}_m / (1-\lambda_p)$), and the inertial forces including added mass ($((C_m\lambda_p/(1-\lambda_p))\partial \hat{U}_m/\partial t$), with C_m the inertial force coefficient. These three forces are characterized by the following length scales, respectively, the shear length scale,

$$L_S = h_v \left(\frac{U_\infty}{u_{*hv}}\right)^2 = \frac{2h_v}{C_f}, \tag{4}$$

where $C_f = 2(u_{*hv}/U_\infty)^2$ is the meadow friction factor, the drag length scale,

$$L_D = \frac{2h_v(1-\lambda_p)}{C_D\lambda_f}, \tag{5}$$

and the oscillation length scale, which is simply the wave orbital excursion, $A_\infty = U_\infty/\omega$ above the meadow.

[10] Conceptually, the drag and shear length scales describe the scale at which the effects of drag and shear begin to influence fluid motion. With these forces, the governing equation becomes [*Lowe et al.*, 2005a]

$$\frac{\partial(\hat{U}_m - U_\infty)}{\partial t} = \frac{|U_\infty|U_\infty}{L_S} - \frac{|\hat{U}_m|\hat{U}_m}{L_D} - \left(\frac{C_m\lambda_p}{1-\lambda_p}\right)\frac{\partial \hat{U}_m}{\partial t}. \tag{6}$$

By introducing the complex variables $\hat{U}_m = \mathrm{Re}\{\beta A_\infty \omega e^{i\omega t}\}$ and $U_\infty = \mathrm{Re}\{A_\infty \omega e^{i\omega t}\}$, and considering only the first Fourier harmonic, we suggest simplifying equation (6), after some straightforward algebra, to

$$i(\beta - 1) = \frac{8}{3\pi}\frac{A_\infty}{L_S} - \frac{8}{3\pi}\frac{A_\infty}{L_D}|\beta|\beta - i\left(\frac{C_m\lambda_p}{1-\lambda_p}\right)\beta. \tag{7}$$

To obtain this result, we assume that A_∞ is real and positive while β may be complex. The ratio of in-canopy velocity to the velocity above the canopy is simply $\alpha = |\beta|$.

[11] From equation (7), we see that if the wave excursion is smaller than the drag and shear length scales ($A_\infty \ll L_S$ and L_D), the wave motion is unaffected by the drag and shear stress, and the flow is dominated by inertia. At this limit, the velocity ratio is given by the following, with subscript i used to emphasize inertia-dominated conditions [*Lowe et al.*, 2005a],

$$\alpha_i = \frac{1-\lambda_p}{1+(C_m-1)\lambda_p}. \tag{8}$$

At the other limit of flow behavior, when the wave excursion, A_∞, is much longer than L_S and L_D, the flow resembles a current. At this limit, the inertial forces drop out, as the acceleration term is negligibly small. Flow within the meadow is determined by the balance of shear and drag forces. Using subscript c to denote the current-only limit, as in the study by *Lowe et al.* [2005a], we have the following velocity ratio:

$$\alpha_c = \sqrt{\frac{L_D}{L_S}}. \tag{9}$$

For the intermediate case, where the effects of both drag and inertia are important, equation (7) must be solved iteratively to yield $\alpha = |\beta|$. *Lowe et al.* [2005a] solved equation (6) numerically by providing an initial condition and marching forward in time until a quasi-steady state is achieved. Alternatively, we propose the use of the Fourier decomposition shown in equation (7), which yields identical results for the inertia and current-only limits and can be more easily solved for the general case.

[12] Equation (6) assumes that the drag-generating elements are rigid, which is not the case with our canopy modeled on flexible seagrass. However, incorporating the impact of wave-induced blade movement in a predictive model is extremely difficult and requires the development of a coupled fluid-structure interaction model. On the basis of observations of blade motion, we argue in a companion study (M. Luhar et al., Seagrass blade motion under waves and its impact on wave decay, submitted to *Marine and Ecology Progress Series*, 2010) that a rigid vegetation model is appropriate if an effective rigid canopy height is used. The effective height is defined as the vertical extent of the meadow over which the blades do not move significantly relative to the water. For the wave conditions considered by Luhar et al. (submitted manuscript, 2010), the effective height was typically less than half the blade length. However, in unidirectional flows, there is some relative motion between the blades and the water along the entire blade length [e.g., *Ghisalberti and Nepf*, 2006]. Furthermore, in a recent field study measuring wave decay over seagrass beds, *Bradley and Houser* [2009] observed relative motion along the whole blade in low-energy, broadband wave conditions. For generality, therefore, we will assume that the effective height is equal to the blade length.

2.3. Wave-Induced Current

[13] We propose that the forces generated within the model meadow lead to a nonzero mean (time-invariant) wave stress at the top of the canopy, which drives a mean current through the meadow. The magnitude of this wave stress and the mean flow generated by it can be estimated based on the arguments shown by *Fredsøe and Deigaard*

[1992] for wave boundary layers. Within the meadow, the horizontal wave velocity, $U_{w,m}$, deviates from the linear wave theory solution, U_w (equation (1a)), because of the forces exerted by the vegetation. From continuity, this deviation leads to the generation of a vertical velocity, $W_{w,m}$, in addition to that predicted by linear wave theory. This additional velocity at the top of the meadow ($z = h_v$) can be expressed as

$$W_{w,m}(z=h_v) = -\frac{\partial}{\partial x}\int_0^{h_v}(U_{w,m}-U_w)dz = \frac{k}{\omega}\int_0^{h_v}\frac{\partial}{\partial t}(U_{w,m}-U_w)dz, \tag{10}$$

where the relation between the spatial and temporal derivatives for propagating waves, $\partial/\partial x = -(\omega/k)\partial/\partial t$, is used. Note that the integral on the right-hand side of equation (10) resembles the vertically averaged momentum balance for the meadow shown in equation (6) when multiplied by $(1/h_v)$. Above the meadow, the horizontal oscillatory velocity is described by linear wave theory (U_w; equation (1a)), but the vertical velocity field includes both the velocity predicted by linear theory (W_w; equation (1b)) and the additional vertical velocity, $W_{w,m}$, shown in equation (10). Unlike the linear wave solution, $W_{w,m}$ is not perfectly out of phase with the horizontal oscillatory velocity, leading to a nonzero time-averaged wave stress, $\langle U_w W_{w,m}\rangle$, acting at the top of the meadow.

[14] To estimate the magnitude of this wave stress, we consider the energy balance for the meadow. Wave energy is transferred from the outer flow into the meadow via the work done by the wave-induced pressure at the top of the meadow, $-\langle p_w(W_w + W_{w,m})\rangle$, and the work done by the shear stress at the interface, $\langle \tau_w U_w\rangle$. The energy transfer is balanced by dissipation within the meadow, $\langle E_D\rangle$:

$$-\langle p_w(W_w + W_{w,m})\rangle + \langle \tau_w U_w\rangle = \langle E_D\rangle. \tag{11}$$

Note that $\langle E_D\rangle$ includes dissipation attributed to the forces exerted by the vegetation, dissipation caused by bed stress, and shear-induced viscous dissipation. Above the meadow, we assume the horizontal oscillatory velocity and pressure fields are specified by the linear wave solution; hence, $p_w = \rho(\omega/k)U_w$ as shown in equation (2). Then, equation (11) may be rearranged to yield the time-averaged wave stress at the top of the canopy:

$$\rho\langle U_w W_{w,m}\rangle = \frac{k}{\omega}(\langle \tau_w U_w\rangle - \langle E_D\rangle). \tag{12}$$

Assuming that energy dissipation is dominated by the drag force exerted by the vegetation, f_D, i.e., excluding bed friction and viscous dissipation [see also *Mendez and Losada*, 2004; *Lowe et al.*, 2007; *Bradley and Houser*, 2009; Luhar et al., submitted manuscript, 2010],

$$\langle E_D\rangle = \left\langle \int_0^{h_v} f_D U_m dz \right\rangle, \tag{13}$$

where U_m is the velocity inside the meadow. We ignore the contribution of the inertia force since this tends to be in phase with the flow acceleration, leading to a zero time average when multiplied by the velocity. Furthermore, for typical values of C_f and $C_D a_v h_v$, the energetic contribution of the work done by the shear stress, which is of $O[\rho C_f U_w^3]$, is negligible compared to the total energy dissipation, which is of $O[\rho C_D a_v h_v U_m^3]$. Specifically, for the wave conditions tested here, the magnitude of the in-canopy velocity, U_m, is comparable to the outer flow velocity, U_w (Tables 1 and 2), and C_f is an $O[0.01]$ constant while the parameter $C_D a_v h_v$ is $O[1]$. Under these assumptions, the time-averaged wave stress at the top of the canopy is

$$\rho\langle U_w W_{w,m}\rangle = -\frac{k}{\omega}\left\langle \int_0^{hv} f_D U_m dz \right\rangle. \tag{14}$$

Integrating the momentum equation over the height of the meadow and time averaging leads to the following physically intuitive mean momentum balance [e.g., *Fredsøe and Deigaard*, 1992]:

$$-\rho\langle U_w W_{w,m}\rangle + \langle \tau_w\rangle - \langle \tau_b\rangle = \langle F_D\rangle, \tag{15}$$

where, $\langle \tau_w\rangle$ and $\langle \tau_b\rangle$ are the mean shear stresses at the top of the canopy and at the bed, and

$$\langle F_D\rangle = \left\langle \int_0^{hv} f_D dz \right\rangle, \tag{16}$$

is the time-averaged drag force integrated over the height of the canopy. For simplicity, the $\partial/\partial x$ convective acceleration term, caused by slow wave decay in the x-direction, and the mean pressure gradient have been assumed negligible. Assuming that the mean shear stresses are negligible compared to the vegetation drag, equations (14) to (16) can be combined to yield

$$\frac{k}{\omega}\left\langle \int_0^{hv} f_D U_m dz \right\rangle = \left\langle \int_0^{hv} f_D dz \right\rangle. \tag{17}$$

Recognizing that the velocity inside the canopy, U_m, consists of both an oscillatory ($U_{w,m}$) and a mean flow ($U_{c,m}$) component, the drag force using a standard quadratic law is $f_D = (1/2)\rho C_D a_v |U_{w,m} + U_{c,m}|(U_{w,m} + U_{c,m})$. However, on the basis of experimental results [*Sarpkaya and Isaacson*, 1981] and numerical simulations [*Zhou and Graham*, 2000], the use of a two-term formulation for the drag force is more appropriate in combined wave-current flows. Following *Zhou and Graham* [2000], we decompose the drag force into its steady and time-varying components with separate drag coefficients, C_{Dc} and C_{Dw} respectively, for each term,

$$f_D = f_{Dc} + f_{Dw} = \frac{1}{2}\rho C_{Dc} a_v U_{c,m}{}^2 + \frac{1}{2}\rho C_{Dw} a_v |U_{w,m}| U_{w,m}. \tag{18}$$

Both drag coefficients, C_{Dw} and C_{Dc} [e.g., *Zhou and Graham*, 2000] depend on the Reynolds number ($Re = U_w d/\nu$, where d is a typical length scale for the drag-generating elements), the Keulegan-Carpenter number ($KC = U_w T/d$, where T is the wave period), and the ratio of

Table 1. Wave and Vegetation Parameters for Each Experiment[a]

Run	n_s (cm^{-2})	H (cm)	T (s)	a[b] (cm)	A_∞/S	α[c] (z = 1 cm)	α (7)[d]	α_i (8)[d]	Mean (U_c)[c] (cm s^{-1})	z (U_c = 0)[c] (cm)	$U_{c,m}$ (21)[d] (cm s^{-1})	U_s (22)[d] (cm s^{-1})	$U_{R,m}$ (23)[d] (cm s^{-1})
D1	0.03	39	1.4	3.2	0.5	0.95	0.97	0.97	0.5	11.2	2.1	0.8	0.5
D2	0.06	39	1.4	3.1	0.7	0.92	0.94	0.94	0.9	12.7	1.9	0.7	0.3
D3	0.09	39	1.4	3.1	0.8	0.92	0.91	0.92	1.0	13.1	1.9	0.7	0.3
D4[e]	0.12	39	1.4	3.1	1.0	0.94	0.87	0.89	1.8	10.9	1.9	0.7	0.2
D5	0.15	39	1.4	3.0	1.1	0.94	0.84	0.87	1.9	13.3	1.9	0.7	0.2
D6	0.18	39	1.4	2.9	1.1	0.92	0.82	0.84	1.6	14.1	1.8	0.6	0.2
D6[f]	0.18	39	1.4	3.1	1.2	0.79	0.81	0.84	1.9	11.1	2.0	0.7	0.2
H1	0.12	16	1.4	0.9	0.6	0.95	0.89	0.89	0.3	5.2	1.0	0.2	0.5
H2	0.12	24	1.4	1.7	0.8	0.94	0.88	0.89	0.8	9.0	1.5	0.4	0.3
H3	0.12	32	1.4	2.4	0.9	0.93	0.88	0.89	1.4	9.2	1.7	0.5	0.3
H4[e]	0.12	39	1.4	3.1	1.0	0.94	0.87	0.89	1.8	10.9	1.9	0.7	0.2
T1	0.12	39	0.9	2.8	0.4	0.93	0.89	0.89	0.4	1.9	0.7	0.7	0.2
T2	0.12	39	1.1	3.3	0.7	0.92	0.88	0.89	1.1	9.1	1.6	0.9	0.3
T3[e]	0.12	39	1.4	3.1	1.0	0.94	0.87	0.89	1.8	10.9	1.9	0.7	0.2
T4	0.12	39	2.0	3.2	1.6	0.89	0.85	0.89	2.2	13.4	2.5	0.7	0.3
A1	0.12	39	1.4	0.8	0.2	0.94	0.89	0.89	0.1	1.7	0.3	0.0	0.0
A1[f]	0.12	39	1.4	0.8	0.3	0.92	0.89	0.89	0.1	4.9	0.3	0.0	0.0
A2	0.12	39	1.4	1.7	0.5	0.95	0.89	0.89	0.4	10.2	0.8	0.2	0.1
A3[e]	0.12	39	1.4	3.1	1.0	0.94	0.87	0.89	1.8	10.9	1.9	0.7	0.2
A4	0.12	39	1.4	4.3	1.4	0.94	0.86	0.89	3.3	12.0	3.2	1.4	0.5
A5	0.12	39	1.4	5.2	1.6	0.91	0.85	0.89	4.2	11.9	4.2	2.0	0.6
A5[f]	0.12	39	1.4	5.3	1.7	0.80	0.85	0.89	4.3	12.2	4.3	2.1	0.6
	(0.003)	(0.5)	(0.05)	(0.2)	(0.1)	(0.03)	(0.01)	(0.01)	(0.3)	(0.5)	(0.1)	(0.1)	(0.05)

[a]The values shown in the last rows represent typical experimental uncertainty.
[b]The wave amplitude was calculated by fitting the linear theory solution (1a) to measured oscillatory velocities at the highest four measurement locations ($z \geq 21$ cm). Exceptions are runs H3, where the top three measurements were used, and runs H1 and H2, for which the top two measurements were used.
[c]Indicates measurements from experiment.
[d]Indicates equations used to arrive at the predicted values.
[e]Identical runs; listed in multiple locations for clarity.
[f]Repeats with wooden dowels left in place in the clearing.

mean to oscillatory velocity. However, the two coefficients are typically of comparable magnitude.

[15] Substituting (18) into (17) and time averaging under the assumption that the parameters C_{Dc}, C_{Dw}, and a_v are constants leads to

$$\frac{k}{\omega}\int_0^{hv}\frac{1}{2}\rho a_v\left(C_{Dc}U_{c,m}{}^3+C_{Dw}\frac{4}{3\pi}u_{w,m}{}^3\right)dz=\int_0^{hv}\frac{1}{2}\rho C_{Dc}a_vU_{c,m}{}^2dz, \tag{19}$$

where $u_{w,m}$ is the magnitude of the in-canopy oscillatory flow, $U_{w,m} = u_{w,m}\cos(\omega t)$. The mean current is a second-order phenomenon, generated because of nonlinear interaction between the oscillatory velocities. As a result, $U_{c,m} \ll u_{w,m}$. Then, assuming C_{Dw} and C_{Dc} are of comparable magnitude, the energy dissipation within the meadow is dominated by the oscillatory drag force and

$$\frac{k}{\omega}\int_0^{hv}\frac{1}{2}\rho a_v\left(C_{Dw}\frac{4}{3\pi}u_{w,m}{}^3\right)dz=\int_0^{hv}\frac{1}{2}\rho C_{Dc}a_vU_{c,m}{}^2dz. \tag{20}$$

Given that the model seagrass blades are vertically uniform (see section 3) and that the parameter $\cosh kh_v$, which is the ratio of the horizontal oscillatory velocity at the top of the canopy to that at the bed (equation (1a)), is smaller than 1.2 for all the cases tested here, we ignore any vertical variation in a_v, C_{Dw}, C_{Dc}, and $u_{w,m}$. For simplicity, we also assume $U_{c,m}$ to be constant over the height of the meadow and solve equation (20) to obtain an estimate for the mean-current generated within the meadow,

$$U_{c,m}=\sqrt{\frac{4}{3\pi}\frac{C_{Dw}}{C_{Dc}}\frac{k}{\omega}u_{w,m}{}^3}. \tag{21}$$

Equation (21) indicates that the magnitude of the mean current is controlled primarily by wave parameters (k, ω, and $u_{w,m}$) and does not depend on the canopy parameters (h_v or a_v). However, below we discuss how the conditions under which (21) applies is dependent on the ratio of blade spacing and wave excursion (i.e., it will have some dependence on a_v). In addition to the wave conditions, an important

Table 2. Observed and Predicted Velocity Ratio for Unidirectional Flow Over Seagrass Model[a]

Run	h_v (cm)	$\langle C_Da_v\rangle$ (cm^{-1})	u^*_{hv}/U_{hv}	C_f[b]	$\hat{U}_m/U_\infty$	α_c (9)[c]
F1	21.5	0.064	0.20	0.08	0.22	0.25
F2	21.3	0.060	0.17	0.06	0.23	0.21
F3	20.0	0.047	0.17	0.06	0.22	0.24
F4	18.6	0.045	0.18	0.06	0.23	0.27
F5	17.0	0.040	0.15	0.05	0.26	0.26
F6	15.5	0.034	0.14	0.04	0.28	0.27
	(0.5)	(0.003)	(0.02)	(0.01)	(0.01)	(0.01)

[a]Data are from *Ghisalberti and Nepf* [2006]. Run numbers follow convention used by the above authors. The last row in the table indicates typical uncertainty.
[b]Estimated based on $Cf = 0.5\ (u^*_{hv}/U_{c,hv})^2$.
[c]Indicates equation used.

quantity governing the magnitude of the mean current is the ratio of drag coefficients, C_{Dw}/C_{Dc}. *Zhou and Graham* [2000] performed numerical simulations estimating the force acting on a single circular cylinder in combined wave-current flows. Simulation results for $U_c/U_w = 0.25$ showed the drag coefficient ratio to decrease from $C_{Dw}/C_{Dc} \approx 1.8$ for $KC = 0.2$ ($Re = 40$) to $C_{Dw}/C_{Dc} \approx 0.5$ for $KC = 26$ ($Re = 5200$), with Re and KC based on cylinder diameter. For the experimental conditions considered here, the Keulegan-Carpenter number, based on blade width and near-bed orbital velocity, ranges from $KC \approx 14$ ($Re \approx 90$) to $KC \approx 94$ ($Re \approx 590$). If the stem diameter is used instead of blade width (see section 3), which might be more appropriate near the base of the model plants used for the experiments, the ranges are $KC \approx 5.8$–39 ($Re \approx 220$–1400). Given the overlap in range between the experiment conditions considered here, and the numerical simulations performed by *Zhou and Graham* [2000], it is reasonable to assume that C_{Dw}/C_{Dc} is an $O[1]$ parameter.

2.4. Return Current

[16] The preceding analysis considers wave-induced oscillatory and mean flow at a fixed point (i.e., an Eulerian perspective). However, it is well known that even for purely oscillatory wave motion, individual water parcels (i.e., a Lagrangian perspective) tend to drift in the direction of wave propagation. This phenomenon is called Stokes' drift [see *Fredsøe and Deigaard*, 1992 for a discussion]. Because the flume is a closed system, mass transport in the direction of wave propagation, attributed to both the wave-induced mean current described above and the Stokes' drift, sets up a surface slope. The pressure gradient caused by this surface setup drives a return current, leading to zero depth-averaged net transport. This return current may modify the measured meadow drift, relative to the theoretical prediction derived above. To estimate the magnitude of this return current, we assume that the flow field attributed to the pressure gradient can simply be superimposed onto the existing wave-induced oscillatory and mean velocity fields. Most of the return current will be diverted above the meadow because of canopy drag. We assume that the ratio of the return current within the meadow ($U_{R,m}$) to the return current above the meadow (U_R) is given by the parameter α_c, shown in equation (9). The depth-integrated Stokes' drift (per unit width) is

$$Q_s = U_s h = \frac{1}{2}\frac{a^2\omega}{\tanh(kh)} \tag{22}$$

[e.g., *Fredsøe and Deigaard*, 1992], where U_s is the depth-averaged mass transport velocity attributed to Stokes' drift. We can now write the following mass balance,

$$Q_s + U_{c,m}h_v = U_R(h - h_v) + U_{R,m}h_v, \tag{23}$$

from which we can estimate the return current within the meadow, $U_{R,m} = a_c U_R$. Experimental results reported later (Table 1) suggest that, for most cases, the impact of the return current within the meadow is negligible.

3. Methods

[17] The experiments were performed in a 24 m long, 38 cm wide, and 60 cm deep flume equipped with a paddle-type wave maker. The vertical paddle was actuated using a hydraulic piston driven by a Syscomp WGM-101 arbitrary waveform generator. The waveform generator was programmed to produce surface waves of the desired amplitude and frequency based on the closed-form solution for paddle motion described by *Madsen* [1971]. A plywood beach of slope 1:5 and covered with rubberized coconut fiber limited reflections to less than 10% of the incident wave. The model canopy was 5 m long. The canopy comprised model plants placed in four predrilled baseboards 1.25 m long. Two additional baseboards were placed both upstream and downstream of the model vegetation to ensure a uniform bed roughness across the test section. Each model plant consisted of six polyethylene (density $\rho_b = 920$ kg m^{-3}; elastic modulus $E = 3 \times 10^8$ Pa) blades of length $l_b = 13$ cm, width $w_b = 3$ mm, and thickness $t_b = 0.1$ mm attached to a 2 cm long wooden dowel of 0.64 cm diameter using rubber bands. With the rubber bands in place, the maximum diameter of the dowels was distributed with a mean of 0.92 cm and a standard deviation of 0.03 cm. Where necessary, a mean stem diameter, $d = 0.78$ cm, is used. When inserted into the baseboard, the stem (dowel) protruded 1 cm above the bed.

[18] Velocity measurements were made with a 3-D Acoustic Doppler Velocimeter (ADV; Nortek Vectrino). Synchronous measurements of the wave height were made at the same x-location using a wave gauge of 0.2 mm accuracy. The analog output from the wave gauge was amplified and logged to a computer using an analog-digital converter (NI-USB6210, National Instruments). Both the ADV and wave gauge were mounted on a trolley moving on precision rails. Vertical profiles of velocity were measured at two longitudinal locations, midway through the canopy and upstream of the canopy. The model bed was shifted longitudinally along the flume to ensure that the measurement location midway through the canopy corresponded to an antinode of the partially standing waves created by reflections from the downstream end of the flume. The other measurement location was chosen to be an antinode at least half a wavelength upstream of the canopy. This eliminates the lower-order spatially periodic variation in wave and velocity amplitude associated with the 10% reflection. Velocities were measured at 1 cm vertical intervals. At each location, velocities and surface displacement were measured for 6 min at 25 Hz. The height of the lowest measurement location varied between 0.1 and 0.9 cm above the bed ($z = 0$).

[19] A schematic of the setup is shown in Figure 1. Wave period ($T = 0.9$–2.0 s) and amplitude ($a = 0.8$–5.3 cm), water depth ($h = 16$–39 cm), and vegetation density ($n_s = 300$–1800 stems m^{-2}, or $n_b = 1800$–$10{,}800$ blades m^{-2}) were varied systematically. These parameter ranges were chosen based on typical field values for the dimensionless parameters a/h, kh, h_v/h, and $a_v h_v$ (see Luhar et al. [submitted manuscript, 2010] for details). The conditions for each experimental run are shown in Table 1. To measure velocities close to the bed within the meadow, all vegetation was removed from a circular area approximately 10 cm in diameter, which was the minimum cleared area necessary to prevent blades from entering the measurement control volume. To test whether the clearing had an appreciable impact on the velocity structure near the bed, three runs were repeated with the wooden dowels (with rubber bands but no

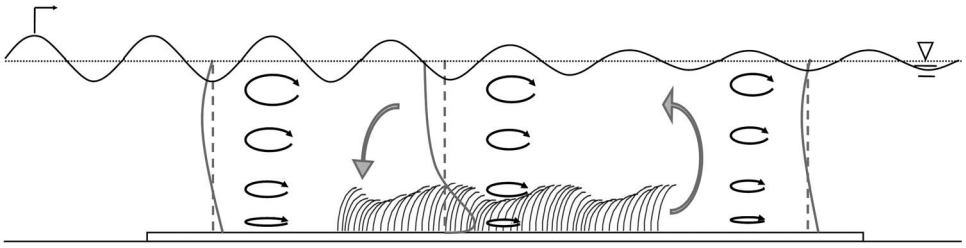

Figure 2. Qualitative overview of the flow pattern at the meadow scale. The decay in wave height (fine black line) along the meadow results in a proportional decrease in the oscillatory velocity fields. The black ellipses with arrows indicate the wave orbitals. Vertical profiles of the mean current (heavy gray lines) are shown at an upstream, downstream, and in-meadow position. At each position, the vertical dashed lines indicate the axis position for the profile. The local circulation pattern, shown by the large gray arrows, results from the difference in the velocity profile within and outside the meadow. The direction of wave propagation is from left to right. Not to scale.

blades attached) replaced in the cleared area. These runs are marked with a superscript "f" in Table 1. The dynamic influence of this cleared area on both unsteady and steady velocity components is discussed below.

[20] The velocity measurements were decomposed into mean (U_c, W_c), root-mean-square (RMS) oscillatory ($U_{w,RMS}$, $W_{w,RMS}$), and turbulent (u', w') components using a phase-averaging technique. The velocity readings were binned into different phases based on the upward zero-crossings ($\varphi = 0$ rad) of the synchronous wave elevation measurements. Wave elevation is defined as the instantaneous surface displacement minus the mean water level. The wave crest and wave trough correspond to $\varphi \approx \pi/2$ rad and $\varphi \approx 3\pi/2$ rad, respectively. The velocity measurements for each phase bin where then ensemble averaged for the entire record (180–396 waves, depending on frequency) to yield the phase-averaged velocity values ($u(\varphi)$, $w(\varphi)$). The mean and RMS velocity components were then calculated by performing the following operations (only the u-component is shown for brevity):

$$U_c = \frac{1}{2\pi}\int_0^{2\pi} u(\varphi)d\varphi, \tag{24}$$

and

$$U_{w,RMS} = \sqrt{\frac{1}{2\pi}\int_0^{2\pi} (u(\varphi) - U_c)^2 d\varphi}. \tag{25}$$

Similarly, the turbulent Reynolds stress, $u'w'$ (φ), was calculated by subtracting the phase-averaged velocities from the instantaneous velocities, multiplying the vertical and horizontal components, and ensemble-averaging over all data within that phase bin. The time-averaged turbulent Reynolds stress (as before $\langle\cdot\rangle$ denotes a time average.) was then calculated as

$$\langle u'w'\rangle = \frac{1}{2\pi}\int_0^{2\pi} u'w'(\varphi)d\varphi. \tag{26}$$

4. Results

[21] A qualitative overview of the observations at the scale of the entire bed is presented in Figure 2. Upstream of the model seagrass bed, we observe very little wave decay (less than 1.5% decrease in wave height per wavelength), which is due to viscous dissipation at flume bed and walls [e.g., *Hunt*, 1952]. The RMS oscillatory velocities match predicted values based on linear wave theory. A small mean flow is generated close to the bed; the magnitude of this mean current is in reasonable agreement with the *Longuet-Higgins* [1953] solution for induced drift in laminar wave boundary layers.

[22] As an example, the velocity measurements shown in Figures 3a–3c, made upstream of the meadow for run A5, support this qualitative description of the velocity structure. The RMS oscillatory velocities are predicted to within 5% by linear wave theory (Figure 3a), and the mean velocity is maximum at the measurement position closest to the bed ($z = 0.4$ cm, $U_c = 2.4$ cm/s) (Figure 3b). The magnitude of this mean current is consistent with the laminar boundary layer solution shown in equation (3), which predicts that the induced drift will be $U_c = 1.9$ cm/s outside the wave boundary layer. For laminar flows, the boundary layer thickness is $O[(\nu/\omega)^{1/2}] \sim 0.05$ cm. Over a smooth bottom, the boundary layer transitions from laminar to turbulent for a wave Reynolds number, $Re_w = U_\infty A_\infty/\nu > 5 \times 10^4$ [e.g., *Fredsøe and Deigaard*, 1992]. For the wave conditions tested here, $Re_w \leq 10{,}000$. Hence, we expect the bottom boundary layer to remain laminar upstream of the canopy.

[23] Figure 3c shows that the turbulent Reynolds stress is essentially zero within uncertainty throughout the water column upstream of the canopy, as expected for linear waves. Note that the Reynolds stress measurements at heights $z = 8.4$ and 9.4 cm (Figure 3c) are not reliable because these locations correspond roughly to the "weak spots" of the ADV (Nortek Forum data are available at http://www.nortek-as.com/en/knowledge-center/forum/velocimeters/30180961; last accessed on 29 March 2010). At this height, acoustic reflections from the bed interfere with the signal from the measurement volume, resulting in occasional spikes in both the horizontal and vertical components of velocity. We observe that the spikes tend to be more frequent during set phases of the wave cycle, resulting in a coherent bias of the $\langle u'w'\rangle$ estimate. To summarize, for the measurement location upstream of the meadow, the linear wave solution coupled with laminar boundary layer theory describes the velocity structure well.

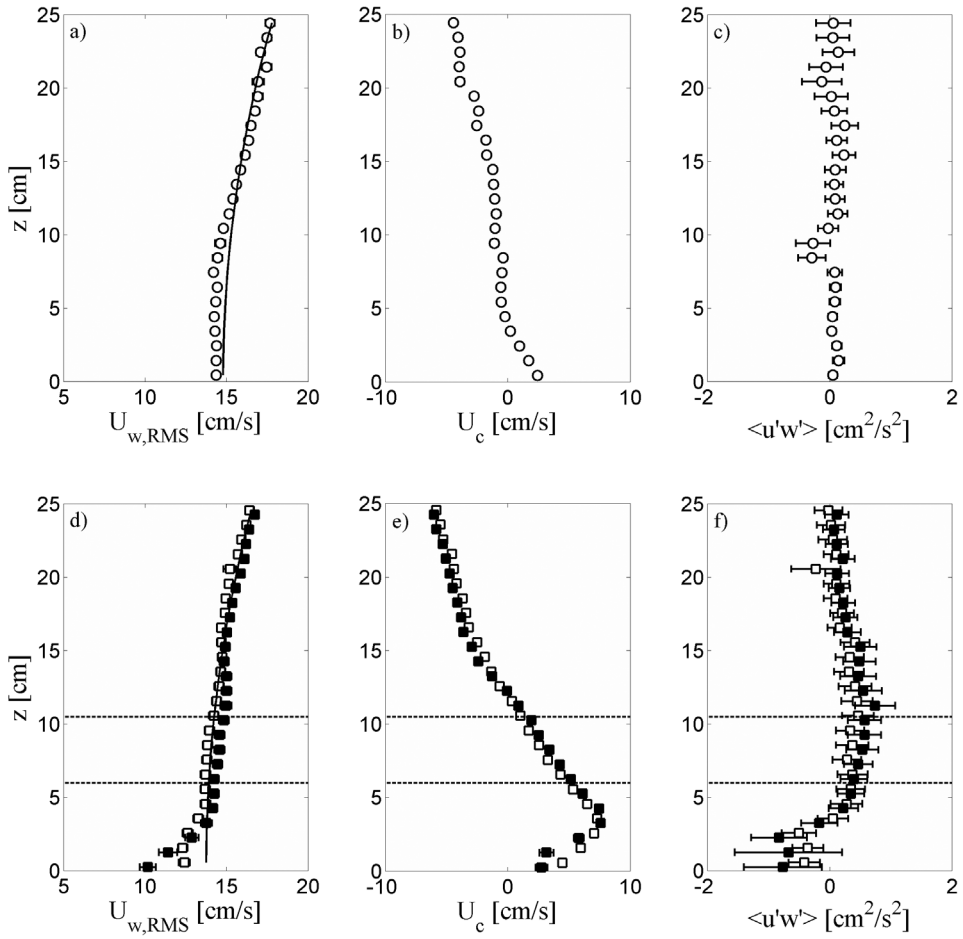

Figure 3. Vertical profiles of RMS wave velocity, mean velocity, and Reynolds stress for run A5. Figures 3a–3c correspond to the measurement location upstream of the meadow. Figures 3d–3f show profiles for the measurement location within the meadow. Results for the case in which a 5 cm radius circle was completely cleared of vegetation are plotted as white squares. Black squares represent the case in which wooden dowels were left in this clearing and only blades were removed. Solid lines in Figures 3a and 3d represent RMS velocity profiles predicted by linear wave theory (equation (1a)). The horizontal dashed lines in Figures 3d–3f show the estimated maximum and minimum canopy heights over a wave cycle. The bottom line shows the canopy height under a wave crest, when the blades tend to lie streamwise, while the top line shows the canopy height under a wave trough, when the model blades are more upright.

[24] In contrast to the observations upstream of the meadow, wave decay is significant over the model seagrass bed (as much as 13% per wavelength for a water depth of 39 cm and 27% per wavelength for a water depth of 16 cm [see Luhar et al., submitted manuscript, 2010]). Furthermore, a mean current in the direction of wave propagation is generated within the model meadow, as shown schematically in Figure 2. This mean current is stronger and extends over a larger vertical distance than the boundary layer drift observed upstream of the meadow. Qualitative observations using a passive tracer (food coloring) indicate that the mean current is established within ~50 cm of the start of the meadow and persists for a similar distance downstream of the meadow, beyond which the velocity structure resembles the observations made upstream of the meadow. The mean current induced within the meadow results in the local circulation pattern, indicated by large gray arrows in Figure 2.

[25] The schematic of in-meadow velocity structure shown in Figure 2 is supported by the measurements shown in Figure 3. Vertical profiles of the RMS orbital velocity, the mean current, and the turbulent Reynolds stresses for run A5 are shown in Figures 3d–3f, respectively. The RMS oscillatory velocity is reduced relative to predictions based on linear theory below $z \approx 4$ cm. For the 10 cm clearing completely devoid of model vegetation, the RMS orbital velocity is reduced to 91% of the predicted linear wave velocities at the lowest measurement location ($z = 0.6$ cm) (Figure 3d, white squares). However, with the stems left in the clearing, the RMS orbital velocity is reduced to 73% of the value predicted by linear wave theory at $z = 0.3$ cm (Figure 3d, black squares). The presence of wooden dowels in the clearing leads to an additional reduction (91% to 73%) in the RMS orbital velocity for $z \leq 1$ cm, suggesting that our

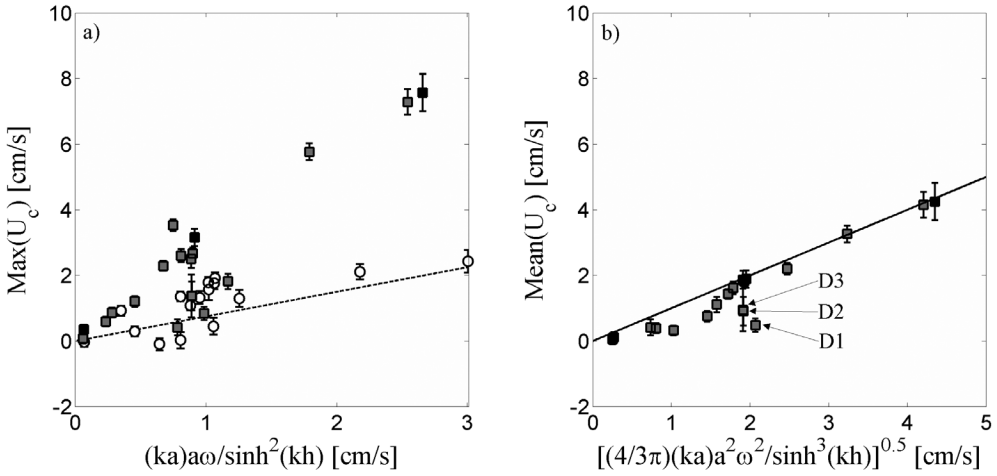

Figure 4. Measured mean currents plotted against theoretical predictions. (a) Comparison of the maximum mean currents, Max(U_c), with the current induced in laminar boundary layers. White circles represent upstream measurements, gray squares indicate in-canopy measurements for the complete clearing, and black squares represent repeat in-canopy measurements with the model stems left in place. The dashed line represents the theoretical value shown in equation (3). (b) Comparison of the canopy-averaged measured current, Mean(U_c), with the theoretical prediction (solid line) shown in equation (21) assuming $u_{w,m} = a\omega/\sinh(kh)$, and $C_{Dw}/C_{Dc} = 1$. Gray and black squares are as described for Figure 4a. Note the different x-axis scales in Figures 4a and 4b.

measurements within the meadow underestimate the reduction of RMS velocity because of the clearing.

[26] Importantly, note that the presence or absence of model stems within the clearing does not affect the mean current significantly, as shown in Figure 3e. The maximum measured mean current is $U_c = 7.3$ cm/s for the complete clearing and $U_c = 7.6$ cm/s with the stems left in place; these values agree within experimental uncertainty. The mean current recorded at the lowest measurement location is close to that predicted for a laminar boundary layer. The magnitude of this mean current increases away from the bed and is greatest at approximately the elevation for which the RMS velocity begins to deviate from linear wave theory ($z \approx$ 4 cm in Figure 3d). Because the flume is a closed system, a return current develops above the meadow ($z > 13$ cm in Figure 3e). Vertical profiles of the turbulent Reynolds stress are physically consistent with the profiles of mean velocity (Figure 3f). The turbulent stress is opposite in sign to $\partial U_c/\partial z$, and it crosses zero at the same height as $\partial U_c/\partial z \approx 0$ (Figures 3e and 3f).

[27] Figure 4a compares the maximum mean current measured upstream of (white markers), and within (gray and black markers), the canopy with the predicted mean velocity for laminar boundary layers, given in equation (3). Consistent with Figure 3b, the maximum measured currents upstream of the canopy agree reasonably well with predicted values for boundary layers. However, the currents generated within the meadow can be 3–4 times larger than the laminar boundary layer prediction. The simple theory developed earlier (equation (21); Figure 4b, solid line) gives a better prediction of the measured in-canopy currents. Note that equation (3) predicts the maximum current outside the boundary layer, whereas equation (21) predicts the vertically averaged mean flow in the seagrass meadow. To reflect this, the maximum measured mean current, Max(U_c), is plotted in Figure 4a, while the canopy-averaged mean current, Mean(U_c), is plotted in Figure 4b. Mean(U_c) is defined as the vertical average of the measured mean flow profile below the zero crossing for U_c (e.g., $z \leq 13$ cm in Figure 3e).

[28] To arrive at a prediction for in-canopy currents using equation (21), the following assumptions are made: the in-canopy oscillatory velocity is equal to the near-bed velocity predicted by linear wave theory, $u_{w,m} = a\omega/\sinh(kh)$, and the ratio of drag coefficients is $C_{Dw}/C_{Dc} = 1$. Under these assumptions, equation (21) simplifies to $U_{c,m} = [(4/3\pi)(ka)a^2\omega^2/\sinh^3(kh)]^{1/2}$. The use of the near-bottom oscillatory velocity in equation (21) is justified because the increase in horizontal oscillatory velocities over the height of the canopy is modest. As mentioned earlier, the ratio of the oscillatory velocity at the top of the canopy to the near-bed velocity based on linear theory (1a) is smaller than 1.2 for all the cases tested here. Furthermore, vegetation resistance only leads to a limited reduction of in-canopy oscillatory velocities as discussed below. The drag coefficient ratio $C_{Dw}/C_{Dc} = 1$ is chosen based on the range suggested by *Zhou and Graham* [2000], $C_{Dw}/C_{Dc} \approx 0.5$–1.8.

[29] For cases D1–D3 (Figure 4b), the observed mean current is significantly lower than the values predicted by equation (21). These cases correspond to the lowest stem densities (n_s in Table 1) tested here. Deviation at the lowest stem densities is not surprising, as the drift must transition back to the boundary layer drift below some threshold density. Figure 4b also suggests that equation (21) overpredicts the mean current for the cases with smaller wave orbital excursions (i.e., small $a/\sinh(kh)$). It is tempting to attribute this overprediction to a variation in the drag coefficient ratio, C_{Dw}/C_{Dc}, based on *KC* and *Re*. However, the simulations performed by *Zhou and Graham* [2000] (see section 2) showed that the drag coefficient ratio, C_{Dw}/C_{Dc}, is highest for low *KC* and *Re*, suggesting that the mean current

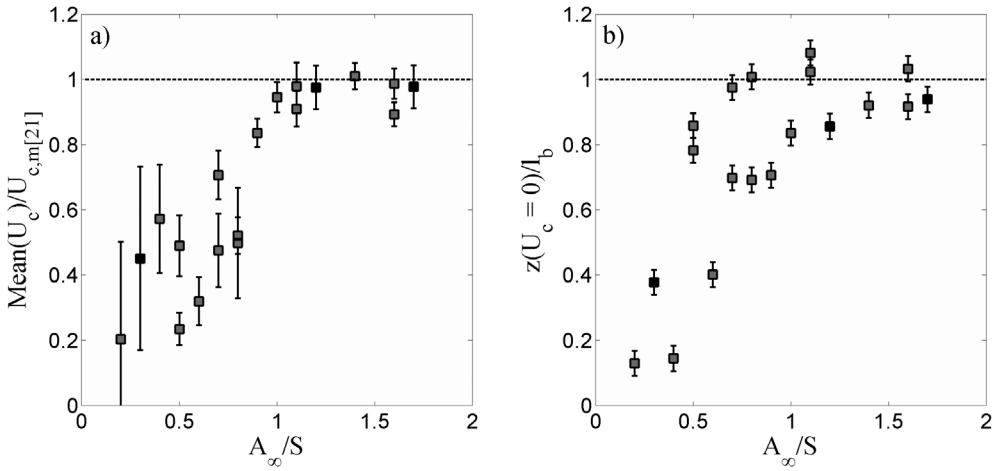

Figure 5. (a) Canopy-averaged mean current normalized by the theoretical prediction, $U_{c,m} = [(4/3\pi)(C_{Dw}/C_{Dc})(ka)a^2\omega^2/\sinh^3(kh)]^{1/2}$, plotted against the ratio of orbital excursion to stem center-center spacing, A_∞/S. C_{Dw}/C_{Dc} is assumed to be 1. (b) Vertical elevation for the zero crossing in the mean current, $z(U_c = 0)$, normalized by the blade length, l_b, plotted against A_∞/S. In both panels, gray squares indicate in-canopy measurements for the runs where a clearing was made for ADV access, and black squares represent repeat in-canopy measurements with the model stems left in place.

should be under-predicted by $C_{Dw}/C_{Dc} = 1$ for waves with smaller orbital velocities and excursions. Clearly, variations in drag based on *KC* and *Re* do not explain the observations.

[30] We suggest that the ratio of orbital excursion, A_∞, to stem center-center spacing, $S = n_s^{-1/2}$, dictates the transition between boundary layer drift and canopy-induced current. This is confirmed by Figure 5a, which shows the observed canopy-averaged mean currents normalized by the predicted values plotted against the ratio A_∞/S. The observed velocity matches the predictions very well for $A_\infty/S \geq 1$, whereas equation (21) overpredicts Mean(U_c) for $A_\infty/S < 1$. The vertical extent over which the mean flow is positive within the canopy, $z(U_c = 0)$, is also a function of A_∞/S (Table 1 and Figure 5b). The height $z(U_c = 0)$ is roughly equal to the blade length for $A_\infty/S \geq 1$ but is smaller than the blade length for $A_\infty/S < 1$, consistent with a transition to boundary layer streaming for $A_\infty/S < 1$. Finally, if we consider only the cases for which $A_\infty/S \geq 1$, the measured profiles collapse to a similar form when normalized by the predicted velocity scale (Figure 6), further confirming the theoretical model. Physically, the large orbital excursions ensure that all the water parcels moving back and forth encounter the model vegetation for $A_\infty/S > 1$. Hence, the bulk representation of seagrass canopy drag used here is accurate. In contrast, for $A_\infty/S < 1$, only the water parcels moving back and forth in the vicinity of the model plants interact with vegetation, and the hydrodynamic impact of the canopy on the wave-induced orbital velocities is diminished. In effect, a bulk representation of canopy drag is strictly valid only for $A_\infty/S \geq 1$. However, if we retain the distributed drag model for simplicity, the wave canopy drag coefficient is reduced for $A_\infty/S < 1$ but not the current drag coefficient, resulting in a lower drag coefficient ratio, C_{Dw}/C_{Dc}.

[31] Finally, we consider the possible impact of the expected return current. In a closed system, a return flow must balance the mass transport in the direction of wave propagation attributed to the wave-induced current ($U_{c,m}h_v$) and Stokes' drift (Q_s). We use equation (23) to estimate the magnitude of the return current within the meadow, $U_{R,m}$ (Table 1). For the cases that satisfy the assumptions of equation (21), $A_\infty/S \geq 1$, the return flow within the meadow is small compared to the measured current. Specifically, $U_{R,m}$ is, at most, 15% of the measured mean current (Table 1). This comparison suggests for $A_\infty/S \geq 1$ that the wave-induced drift within the meadow measured in this study is representative of the magnitudes that will occur in the field (i.e., in the absence of the flume-associated return

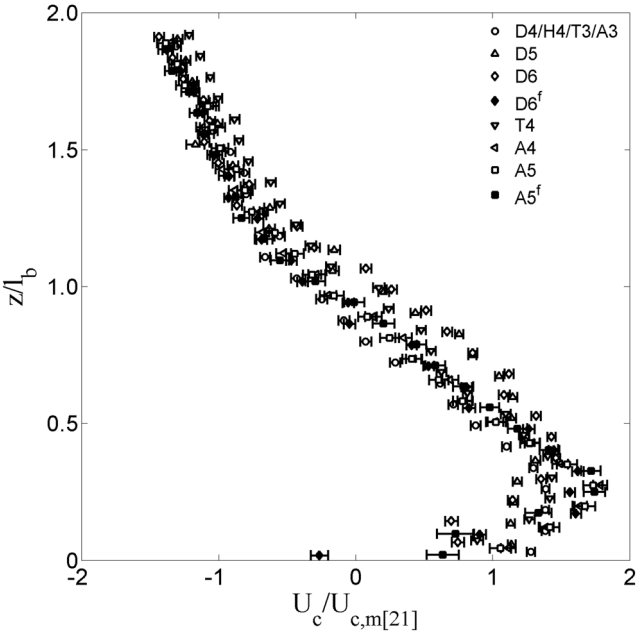

Figure 6. Vertical profiles of measured mean velocity, U_c, normalized by magnitude of the wave-driven current, $U_{c,m}$, predicted by equation (21) for all the runs with $A_\infty/S \geq 1$. The vertical coordinate, z, is normalized by blade length, l_b. Runs are as denoted in the legend.

flow) and that equation (21) needs no adjustment for application in the field.

[32] Next, we consider the reduction in oscillatory velocity within the canopy, which is characterized by the ratio of observed to predicted (from linear theory) horizontal RMS velocity. The velocity reduction is estimated for all cases at $z = 1$ cm. When measurements are not available at $z = 1$ cm, we interpolate linearly between the two lowest velocity measurements. The resulting velocity ratio, α ($z = 1$ cm) is listed in Table 1. Table 1 also lists velocity reductions predicted by equation (8) for the inertia-dominated limit and by the general solution shown in equation (7). The elevation $z = 1$ cm was chosen as the basis for comparison for two reasons. First, velocity reductions were greatest near the bed (see Figure 3d), making the relative uncertainty smaller. Second, the forces exerted by the vegetation for $z > 1$ cm (recall the $z \leq 1$ cm corresponds to the stem region) depend on blade posture and the relative motion between the water and the flexible blades. Predictive quantitative models for blade posture and motion are outside the scope of this study. Since the elevation $z = 1$ cm corresponds to the stem region, the velocity reduction for the inertia-only limit (equation (8)) is calculated using the planar area parameter for the stems, $\lambda_p = n_s \pi d^2/4$. The inertia coefficient is assumed to be $C_m = 2$, as is the case for cylinders. To estimate the velocity reduction using the general solution (equation (7)), we assume the frontal area parameter to be $\lambda_f = n_s d h_s + n_b w_b l_b$, where $h_s = 1$ cm is the height of the stem and l_b is the blade length. Furthermore, we use a drag coefficient, $C_D = 1$, based on the typical values for a cylinder at $Re \geq O[100]$ and a shear coefficient, $C_f = 0.05$, based on velocity and Reynolds stress profiles measured by *Ghisalberti and Nepf* [2006] for a similar model seagrass meadow in unidirectional flow (see Table 2 and discussion below).

[33] As Table 1 shows, for all the wave conditions tested here, there is very little difference between velocity reductions predicted by the general solution, $|\alpha|$ compared to the inertia-dominated limit, α_i. This is in agreement with *Lowe et al.* [2005a], who note that the general solution diverges substantially from the inertia-dominated limit only when the wave excursion to spacing ratio A_∞/S is greater than unity; this ratio is smaller than 2 for all the cases tested here. Consistent with the observation made earlier, the velocity ratio is higher than predicted for most of the cases in which the model vegetation was removed to allow ADV access. The wave-induced flow adjusts locally to the clearing. Hence, the removal of the model vegetation results in higher velocities locally. The exceptions are cases D1–D3, where the observed velocity ratios agree with the predictions within experimental uncertainty. Given the low vegetation densities for these cases, the clearing is not sufficiently distinct from the rest of the sparse meadow. For the cases in which the model stems were left in place in the clearing, agreement between the observed and predicted velocity ratios improves. Given that the smallest velocity ratio we observe is 80% (i.e., a reduction of 20%), the experiments suggest that the reduction in oscillatory velocities within seagrass meadows is limited for wave-dominated conditions, consistent with the assumptions made in predicting the wave-induced mean current.

[34] In contrast, velocities are significantly reduced in similar model seagrass meadows for unidirectional flows [*Ghisalberti and Nepf*, 2006], as shown in Table 2. *Ghisalberti and Nepf* [2006] measured unidirectional velocity profiles over a similar model seagrass meadow of density 230 stems m^{-2} (1380 blades m^{-2}). The shear stress coefficient is estimated using the relation $C_f = 2(u_{*hv}/U_{hv})^2$ shown earlier. Here, $u_{*hv} = [-\langle u'w' \rangle]^{1/2}$ is the friction velocity, and U_{hv} is the unidirectional flow velocity at the top of the meadow, $z = h_v$. Consistent with observations of natural seagrass [e.g., *Grizzle et al.*, 1996], the meadow height decreased with increasing flow speed (Table 2). The compression of blades with increasing flow speed makes the interface with the overflow hydraulically smoother, reducing the friction coefficient of this interface (C_f), a trend that was also noted by *Fonseca and Fisher* [1986]. The blade density considered by *Ghisalberti and Nepf* [2006] is at the lower limit of the conditions used here for the wave experiments (Table 1), yet the velocity ratio, $\hat{U}_m/U_\infty$, is 28% or less (i.e., a reduction of 72% or more). With denser meadows, the reduction will be greater. For a typical dense canopy used here (i.e., 1200 stems m^{-2}, $a_v h_v \approx 2.9$), equation (9) predicts a velocity ratio of $\alpha_c = 0.13$, a velocity reduction of 87%. The implications of these vastly different in-canopy velocities under wave- and current-dominated conditions are discussed in section 5.

5. Discussion

[35] Perhaps the most interesting aspect of this study is the mean current induced within the model seagrass canopy. A significant body of analytical, numerical, and experimental work regarding wave-induced mean currents within laminar and turbulent boundary layers over smooth, rippled, and rough beds already exists (see *Davies and Villaret* [1998, 1999] and *Marin* [2004] for relatively recent reviews). However, to our knowledge, this is the first instance of a similar current being observed within submerged canopies. For field applications, our results suggest that, in addition to wind and tidal forcing, mean currents within submerged canopies can also be induced by wave forcing.

[36] The wave-induced current was established within 50 cm of the upstream edge of the canopy. We propose the following scaling for this development length, L_c. When the mean current is fully developed, the conservation of momentum reduces to a balance between the wave stress and the meadow drag (equation (15)). The balance $\langle U_w W_{w,m} \rangle / h_v = (1/2) C_{Dc} a_v U_{c,m}^2$ leads to $U_{c,m}^2 = 2 \langle U_w W_{w,m} \rangle / C_{Dc} a_v h_v$. Over the development length scale, drag is unimportant, and the wave stress is balanced by the convective acceleration term, $U_{c,m}^2/L_c \sim \langle U_w W_{w,m} \rangle / h_v$. Equating the above expressions leads to the development length $L_c \sim 2/C_{Dc} a_v$, which is consistent with the discussion by *Luhar et al.* [2008]. Given that C_{Dc} is an $O[1]$ parameter, $L_c \sim 2/a_v$. For the vegetation densities tested here, $a_v = 0.054$–0.32 cm^{-1}, leading to $L_c \sim 6.2$–37 cm. Note that this analysis assumes that the wave stress $\langle U_w W_w \rangle$ is set up instantaneously at the upstream edge of the canopy. It is likely that the wave stress develops over a distance on the order of the wave excursion ($A_\infty = 0.7$–4.8 cm for this study). Hence, in order for the mass drift to be generated within a meadow, the meadow must be longer than both the wave excursion and $L_c \sim 2/a_v$. In the field, $a_v \sim 0.01$–

Table 3. Predicted Velocity Reductions for Current- and Wave-Dominated Conditions in the Field for a Range of Seagrass Species[a]

Species		n_b (m^{-2})	l_b (cm)	w_b (cm)	t_b (mm)	λ_f[b]	λp[b]	α_i (8)[c]	α_c (9)[c]	E_{max}[d]	References
P. oceanica	Max[e]	5600	81	0.9	0.8	40.8	0.041	0.68	0.03	4.4	*Pergent-Martini et al.*, 1994;
	Mean	3500	50		0.5	15.8	0.014	0.78	0.06	3.7	*Marbà et al.*, 1996;
	Min	1400	32		0.3	4.0	0.003	0.90	0.11	2.8	*Fourqurean et al.*, 2007
Cymodocea nodosa	Max	6000	30	0.3	1.0	5.4	0.018	0.95	0.10	3.1	*Cancemi et al.*, 2002;
	Mean	3000	17		0.5	1.5	0.005	0.97	0.18	2.3	*Guidetti et al.*, 2002
	Min	1500	10		0.2	0.5	0.001	0.99	0.33	1.7	
Halodule wrightii	Max	30000	20	0.2	0.4	12.0	0.024	0.89	0.06	3.7	*Creed*, 1997, 1999;
	Mean	18000					0.014	0.93			*Fonseca and Bell*, 1998
	Min	6000			10	1.2	0.005	0.98	0.20	2.2	
Ruppia maritima	Max	5700	100	0.2	0.8	8.6	0.007	0.99	0.08	3.6	*Koch et al.*, 2006
	Mean	4800	70		0.6	5.0	0.004	0.99	0.10	3.2	
	Min	3600	40		0.2	2.2	0.001	0.99	0.15	2.6	
T. testudinum	Max	3020	35	1	0.5	10.6	0.015	0.77	0.07	3.3	*Lee and Dunton*, 2000;
	Mean	2400			0.4		0.010	0.80			*Terrados et al.*, 2008
	Min	2000	10		0.4	2.0	0.007	0.83	0.16	2.3	
Zostera marina	Max	3850	80	0.8	0.3	23.1	0.010	0.82	0.05	4.2	*Fonseca and Bell*, 1998;
	Mean	2500	60		0.3	11.3	0.006	0.88	0.07	3.6	*Laugier et al.*, 1999;
	Min	1350	32		0.3	3.2	0.003	0.93	0.12	2.7	*Guidetti et al.*, 2002
Zostera nolti	Max	30000	20	0.2	0.5	9.0	0.021	0.94	0.07	3.5	*Laugier et al.*, 1999;
	Mean	21000	21		0.4	6.6	0.011	0.95	0.09	3.3	*Cabaço et al.*, 2009
	Min	12000	8		0.2	1.4	0.003	0.97	0.19	2.3	
Enhalus acoroides	Mean	137	30	1.5	0.5	0.6	0.001	0.97	0.28	1.8	*Vermaat et al.*, 1995; *Green and Short*, 2003
Halodule uninervis	Mean	7772	10	0.3	0.2	2.3	0.005	0.93	0.15	2.5	*Vermaat et al.*, 1995; *Green and Short*, 2003
Thalassia hemprichii	Mean	2481	20	0.8	0.3	4.0	0.005	0.86	0.11	2.8	*Vermaat et al.*, 1995; *Green and Short*, 2003

[a]An estimate for the maximum mass transfer enhancement factor, $E_{max} = (\alpha_i/\alpha_c)^{1/2}$, is also provided.
[b]Vegetation parameters, $\lambda_f = n_b w_b l_b$ and $\lambda_p = n_b w_b t_b$.
[c]Indicates equation used.
[d]$E_{max} = (\alpha_i/\alpha_c)^{0.5}$, as suggested by *Lowe et al.* [2005b].
[e]Max, maximum; Min, minimum.

0.3 cm^{-1}, leading to $L_c \sim$ 6–200 cm (see Table 3 and also *Luhar et al.* [2008]), while the near-bed wave excursion can be of O[10–500 cm], suggesting that the wave-induced current is likely to exist for seagrass meadows longer than a few meters.

[37] At this point, it must be noted that while the laminar boundary layer theory developed by *Longuet-Higgins* [1953] predicts a mean current in the direction of wave propagation, subsequent experimental and analytical studies [e.g., *Davies and Villaret*, 1998; *Marin*, 2004] show that both the magnitude and direction of the mean current change as the flow transitions from laminar to turbulent. The change in magnitude and direction of the mean current is attributed to the fact that wave asymmetry introduces asymmetries in the turbulence generated near the bed, or the vortices being shed from individual roughness elements. The drag characteristics of the vegetation depend on the periodic shedding and advection of vortices around the plants. Furthermore, qualitative observations of our model meadow indicate (see also Luhar et al., submitted manuscript, 2010) that the induced drift introduces an asymmetry in blade posture, whereby the blades lie streamwise in the direction of wave propagation under the wave crest and remain more upright under the wave trough. The resulting increase in frontal area can lead to greater drag under the wave trough, when the horizontal oscillatory velocity is negative, thereby reinforcing the mean current. Asymmetries in turbulent processes and blade posture can be accounted for by using time-varying drag coefficients in equation (18) (cf. the time-varying eddy viscosity used by *Trowbridge and Madsen* [1984]); however, significant additional experimental and analytical work is required before this can be quantified with any certainty.

[38] The simulations performed by *Zhou and Graham* [2000] were for a cylinder in isolation. For an array of model plants, processes such as wake interaction between neighboring plants could influence the drag coefficients. A combined wave-current flow would also move the wakes back and forth and advect them downstream. To our knowledge, no previous studies have considered this interaction. As a result, we assume that the results obtained by *Zhou and Graham* [2000] for a single cylinder apply to the array of model plants used in this study.

[39] The generation of a mean current within submerged seagrass meadows has important implications for the health of meadows and for the ecologic services provided by the

seagrasses. As mentioned above, the mean current can lead to a bias in blade posture over a wave cycle. Blade posture can control light uptake and, hence, productivity in seagrass meadows [*Zimmerman*, 2003]. The predictive model developed by *Zimmerman* [2003] shows that the fraction of downwelling irradiance absorbed by submerged seagrass meadows increases as the bending angle of the seagrass blades increases. Increased absorption, caused by the increase in horizontal projected leaf area, leads to higher photosynthesis rates until a threshold bending angle of ~20°. Above this threshold, photosynthesis rates decrease because of self-shading; a larger fraction of the incoming light is absorbed in the upper part of the canopy where photosynthesis is no longer limited by light availability.

[40] Notably, the wave-induced current also has the potential to transport sediment and organic matter in the direction of wave propagation. Oscillatory wave velocities can generate turbulence close to the bed and suspend sediment but can only move the suspended sediment back and forth. In contrast, the wave-induced current revealed in this study can advect the material away. Advection could be especially important for fine sediment and organic matter, where the majority of transport is in the form of suspended load. The mean current can also introduce a directional bias in the dispersal of spores, thereby dictating the direction of meadow expansion. Furthermore, the mean currents induced within the meadow may play a role in mediating the economically important nutrient cycling services provided by seagrasses. Nutrient cycling slows down if the rate at which seagrasses extract nutrients from the water is faster than the rate at which the water, and hence nutrients, are replenished within the meadow as a whole. In oscillatory flows, one mechanism of water renewal for seagrass meadows is turbulent exchange with the overlying water column. By systematically flushing the meadow (Figure 2), a wave-induced mean current may provide a second mechanism of water renewal.

[41] The model developed by *Lowe et al.* [2005a] can be used to estimate the velocity reductions expected in field seagrass meadows. Table 3 shows the anticipated velocity ratios for the inertia- and current-dominated limits, α_i and α_c, for a range of real seagrass species. These ratios are estimated using equations (8) and (9) based on the ranges of seagrass blade density (n_b), length (l_b), width (w_b), and thickness (t_b) listed in Table 3. The frontal area parameter is $\lambda_f = n_b w_b l_b$, and the planar area parameter is $\lambda_f = n_b w_b t_b$. The drag and inertia coefficients are assumed to be $C_D = 1$ and $C_f = 0.05$ as before (Tables 1 and 2), whereas the inertia coefficient is simply the ratio of blade width to blade thickness, $C_m = w_b/t_b$ (see discussion in the study by *Vogel* [1994]). As Table 3 indicates, only a few species are likely to experience a significant reduction in in-canopy velocity at the inertia-dominated limit (e.g., *Posidonia oceanica*, α_i = 0.68–0.90); however, at the current-only limit, in-canopy velocities are likely to be reduced by 67% or more for all the species listed (e.g., *P. oceanica*, α_c = 0.03–0.11). Recall that the inertia-dominated limit is applicable when the wave excursion is much smaller than the drag and shear length scales. Because near-bed wave excursions in the field are likely to range from O[10–500 cm], while the drag length scale, $L_D = 2h_v(1 - \lambda_p)/C_D\lambda_f$ is O[5–10 cm] for all the species listed in Table 3, the inertia-dominated limit may not be very relevant for field conditions. For field conditions, therefore, the wave velocity reduction is likely to lie somewhere between the predictions for the inertia-dominated and current-only limits. However, the general conclusion that oscillatory velocities are attenuated less within submerged canopies compared to unidirectional currents remains valid.

[42] The higher magnitude of in-canopy velocities for oscillatory flows relative to comparable unidirectional flows leads to an enhancement of mass transfer at the surface of individual canopy elements [e.g., *Lowe et al.*, 2005b]. Via experiments measuring the rate of dissolution of gypsum blocks, *Lowe et al.* [2005b] confirmed the oft-cited dependence of the convective mass transfer velocity (u_{CT}) on the flow speed within the canopy, $u_{CT} \sim U_m^{1/2}$. *Lowe et al.* [2005b] introduced the "enhancement factor," which is the ratio of mass transfer in oscillatory flow relative to that in unidirectional flow. The maximum possible value for this mass transfer enhancement factor is found in flows at the inertial limit, i.e., $E_{max} = (\alpha_i/\alpha_c)^{1/2}$. This ratio is listed in Table 3 for typical field conditions. Estimates of E_{max} show that convective mass transfer in and out of submerged seagrass meadows may be as much as ~1.7 to ~4.4 times larger for oscillatory flows compared to unidirectional currents of the same magnitude. This is in good agreement with the observations made by *Thomas and Cornelisen* [2003], which show ammonium uptake in a meadow of *Thalassia testudinum* to be ~1.5 times greater in oscillatory flow relative to unidirectional flow. The maximum enhancement predicted for this species of seagrass ranges from ~2.3 to ~3.3 (Table 3).

[43] The weaker damping of in-canopy velocity observed for oscillatory flows compared to mean currents may lead to different horizontal spatial structure within a meadow. In the presence of currents, a meadow can greatly reduce the near-bed velocity, and hence bed stress (e.g., as shown by the typical range of velocity ratios shown in Tables 2 and 3). This can create a feedback that maintains a fragmented meadow structure, as described by *Luhar et al.* [2008]. An isolated patch of seagrass reduces the bed stress within the patch, and the diversion of flow away from the patch enhances the bed stress on the adjacent bare bed. Similarly, flow is enhanced locally within channels cutting through the meadow, inhibiting regrowth and thereby stabilizing the channels [*Temmerman et al.*, 2007]. The scenario is different in wave-dominated conditions, because the meadow does not significantly reduce near-bed wave velocity (and associated bed stress), relative to adjacent bare bed (e.g., as seen in Tables 1 and 3). When a local area of meadow is lost, the bed stress in the bare patch does not increase appreciably, and the vegetation can grow back.

[44] On the basis of this difference in wave- and current-dominated conditions, we anticipate that regions dominated by currents will have more fragmented meadows, because any channels and cuts in the meadow will be maintained by the local adjustment in near-bed flow and bed stress. In contrast, regions dominated by waves will have more uniform vegetation distributions, because under waves, there is little local flow adjustment to the meadow. Some support for the above hypothesis can be found in the field literature. *Fonseca et al.* [1983] observed that as the hydrodynamic

conditions became more current dominated, the meadows became more fragmented. Similarly, *Fonseca and Bell* [1998] measured the percentage of meadow cover across 50 m × 50 m plots and found higher correlations in linear regression between percentage cover and current ($r^2 = 0.60$) than between percentage cover and wave exposure ($r^2 = 0.45$). Using a multiple regression, they found that percentage cover was predominately explained by current ($r^2 = 0.54$) with only a minor contribution from wave exposure ($r^2 = 0.07$).

6. Conclusions

[45] Velocity profiles measured within and above a model seagrass meadow show that a mean current is generated within the meadow under wave forcing. Similar to boundary layer streaming, this mean current is forced by a nonzero wave stress. A simple model, developed in section 2, is able to predict the magnitude of this mean current. By introducing a bias in blade posture, the induced mean current may affect light uptake [*Zimmerman*, 2003] and hence photosynthesis rates. Furthermore, the mean current can play an important role in the net transport of suspended sediment and organic matter. Finally, by continuously renewing the water within the meadow, the induced current may also mediate the ecologically and economically important nutrient cycling services [*Costanza et al.*, 1997] provided by seagrass meadows.

[46] In agreement with *Lowe et al.* [2005a], the velocity reduction within the meadows is lower for oscillatory flows compared to unidirectional flows. The higher in-canopy velocities associated with wave-dominated conditions have been observed to enhance nutrient and oxygen transfer between the seagrasses and the water [*Thomas and Cornelisen*, 2003]. Finally, the limited reduction of in-canopy oscillatory velocities suggests that in wave-dominated regions, the bed stress is not sufficiently distinct in any cuts or channels compared to areas of healthy meadow. Hence, seagrasses may be able to recolonize areas of lost meadow, leading to more uniform meadow structure. This is in contrast to tidal- or current-dominated regions where any cuts or channels tend to be stable because of the local increase in flow and hence bed stress [*Temmerman et al.*, 2007].

[47] **Acknowledgments.** This study received support from the U.S. National Science Foundation under grant OCE 0751358. Any conclusions or recommendations expressed in this material are those of the author(s) and do not necessarily reflect the views of the National Science Foundation. Sylvain Coutu was supported by the Boston-Strasbourg Sister City Association during his stay at MIT, and he thanks the cities of Strasbourg and Boston for making this collaboration possible. Eduardo Infantes thanks the Spanish Ministerio de Ciencia e Innovación (MICINN) FPI scholarship program (BES-2006-12850) for financial support. We also thank Ole Madsen, Amala Mahadevan, and Shreyas Mandre for helpful discussions.

References

Bradley, K., and C. Houser (2009), Relative velocity of seagrass blades: Implications for wave attenuation in low-energy environments, *J. Geophys. Res.*, *114*, F01004, doi:10.1029/2007JF000951.

Cabaço, S., R. Machas, and R. Santos (2009), Individual and population plasticity of the seagrass *Zostera noltii* along a vertical intertidal gradient, *Estuarine Coastal Shelf Sci.*, *82*(2), 301–308, doi:10.1016/j.ecss.2009.01.020.

Cancemi, G., M. C. Buia, and L. Mazzella (2002), Structure and growth dynamics of *Cymodocea nodosa* meadows, *Sci. Mar.*, *66*, 365–373.

Chen, S. N., L. P. Sanford, E. W. Koch, F. Shi, and E. W. North (2007), A nearshore model to investigate the effects of seagrass bed geometry on wave attenuation and suspended sediment transport, *Estuaries Coasts, 30*(2), 296–310.

Costanza, R., et al. (1997), The value of the world's ecosystem services and natural capital, *Nature*, *387*, 253–260, doi:10.1038/387253a0.

Creed, J. C. (1997), Morphological variation in the seagrass *Halodule wrightii* near its southern distributional limit, *Aquat. Bot.*, *59*(1–2), 163–172, doi:10.1016/S0304-3770(97)00059-4.

Creed, J. C. (1999), Distribution, seasonal abundance and shoot size of the seagrass *Halodule wrightii* near its southern limit at Rio de Janeiro state, Brazil, *Aquat. Bot.*, *65*(1–4), 47–58, doi:10.1016/S0304-3770(99)00030-3.

Davies, A. G., and C. Villaret (1998), Wave-induced currents above rippled beds and their effects on sediment transport, in *Physics of Estuaries and Coastal Seas*, edited by J. Dronkers and M. Scheffers, pp. 187–199, Balkema, Brookfield, VT.

Davies, A. G., and C. Villaret (1999), Eulerian drift induced by progressive waves above rippled and very rough beds, *J. Geophys. Res.*, *104*(C1), 1465–1488, doi:10.1029/1998JC900016.

Finnigan, J. (2000), Turbulence in plant canopies, *Annu. Rev. Fluid Mech.*, *32*(1), 519–571, doi:10.1146/annurev.fluid.32.1.519.

Fonseca, M. S., and S. S. Bell (1998), Influence of physical settings on seagrass landscapes near Beauford, North Carolina, USA, *Mar. Ecol. Prog. Ser.*, *171*, 109–121, doi:10.3354/meps171109.

Fonseca, M. S., and J. A. Cahalan (1992), A preliminary evaluation of wave attenuation by four species of seagrass, *Estuarine Coastal Shelf Sci.*, *35*, 565–576, doi:10.1016/S0272-7714(05)80039-3.

Fonseca, M. S., and J. S. Fisher (1986), A comparison of canopy friction and sediment movement between four species of seagrass with reference to their ecology and restoration, *Mar. Ecol. Prog. Ser.*, *29*, 15–22, doi:10.3354/meps029015.

Fonseca, M. S., J. C. Zieman, G. W. Thayer, and J. S. Fisher (1983), The role of current velocity in structuring eelgrass (*Zostera marina* L.) meadows, *Estuarine Coastal Shelf Sci.*, *17*, 367–380, doi:10.1016/0272-7714(83)90123-3.

Fourqurean, J. W., N. Marba, C. M. Duarte, E. Diaz-Almela, and S. Ruiz-Halpern (2007), Spatial and temporal variation in the elemental and stable isotopic content of the seagrasses *Posidonia oceanica* and *Cymodocea nodosa* from the Illes Balears, Spain, *Mar. Biol. Berlin*, *151*, 219–232, doi:10.1007/s00227-006-0473-3.

Fredsøe, J., and R. Deigaard (1992), *Mechanics of Coastal Sediment Transport*, World Sci., Singapore.

Gacia, E., T. C. Granata, and C. M. Duarte (1999), An approach to measurement of particle flux and sediment retention within seagrass (*Posidonia oceanica*) meadows, *Aquat. Bot.*, *65*(1–4), 255–268, doi:10.1016/S0304-3770(99)00044-3.

Ghisalberti, M., and H. M. Nepf (2002), Mixing layers and coherent structures in vegetated aquatic flows, *J. Geophys. Res.*, *107*(C2), 3011, doi:10.1029/2001JC000871.

Ghisalberti, M., and H. M. Nepf (2004), The limited growth of vegetated shear layers, *Water Resour. Res.*, *40*(7), W07502, doi:10.1029/2003WR002776.

Ghisalberti, M., and H. Nepf (2006), The structure of the shear layer in flows over rigid and flexible canopies, *Environ. Fluid Mech.*, *6*, 277–301, doi:10.1007/s10652-006-0002-4.

Granata, T. C., T. Serra, J. Colomer, X. Casamitjana, C. M. Duarte, and E. Gacia (2001), Flow and particle distributions in a nearshore seagrass meadow before and after a storm, *Mar. Ecol. Prog. Ser.*, *218*, 95–106, doi:10.3354/meps218095.

Green, E. P., and F. T. Short (2003), *World Atlas of Seagrasses*, Univ. of Calif. Press, Berkeley.

Grizzle, R. E., F. T. Short, C. R. Newell, H. Hoven, and L. Kindblom (1996), Hydrodynamically induced synchronous waving of seagrasses: Monami and its possible effects on larval mussel settlement, *J. Exp. Mar. Biol. Ecol.*, *206*, 165–177, doi:10.1016/S0022-0981(96)02616-0.

Guidetti, P., M. Lorenti, M. C. Buia, and L. Mazzella (2002), Temporal dynamics and biomass partitioning in three Adriatic seagrass species: *Posidonia oceanica*, *Cymodocea nodosa*, *Zostera marina*, *Mar. Ecol. Berlin*, *23*, 51–67, doi:10.1046/j.1439-0485.2002.02722.x.

Hunt, J. N. (1952), Amortissement par viscosite de la houle sur un fond incline dans un canal de largeur finie, *Houille Blanche*, *7*, 836.

Irlandi, E. A., and C. H. Peterson (1991), Modification of animal habitat by large plants: Mechanisms by which seagrasses influence clam growth, *Oecologia*, *87*, 307–318, doi:10.1007/BF00634584.

Johns, B. (1970), On the mass transport induced by oscillatory flow in a turbulent boundary layer, *J. Fluid Mech.*, *43*, 177–185, doi:10.1017/S0022112070002306.

Kobayashi, N., A. W. Raichle, and T. Asano (1993), Wave attenuation by vegetation, *J. Waterw. Port Coastal Ocean Eng.*, *119*, 30–48, doi:10.1061/(ASCE)0733-950X(1993)119:1(30).

Koch, E. W., and G. Gust (1999), Water flow in tide- and wave-dominated beds of the seagrass *Thalassia testudinum*, *Mar. Ecol. Prog. Ser.*, *184*, 63–72, doi:10.3354/meps184063.

Koch, E. W., L. P. Sandford, S. N. Chen, D. J. Shafer, and J. M. Smith (2006), Waves in seagrass systems: Review and technical recommendations, *U.S. Army Corps of Engineers Tech. Rep. ERDC TR-06-15.p.*, Eng. Res. and Dev. Cent., Alexandria, Va.

Laugier, T., V. Rigollet, and M. L. de Casabianca (1999), Seasonal dynamics in mixed eelgrass beds, *Zostera marina* L. and *Zostera noltii* Hornem., in a Mediterranean coastal lagoon (Thau lagoon, France), *Aquat. Bot.*, *63*, 51–69, doi:10.1016/S0304-3770(98)00105-3.

Lee, K. S., and K. H. Dunton (2000), Effects of nitrogen enrichment on biomass allocation, growth, and leaf morphology of the seagrass *Thalassia testudinum*, *Mar. Ecol. Prog. Ser.*, *196*, 39–48, doi:10.3354/meps196039.

Longuet-Higgins, M. S. (1953), Mass transport in water waves, *Philos. Trans. R. Soc. A*, *245*(903), 535–581, doi:10.1098/rsta.1953.0006.

Longuet-Higgins, M. S. (1958), The mechanics of the boundary-layer near the bottom in a progressive wave, *Proceedings of the 6th International Conference on Coastal Engineeering*, pp. 184–193, Am. Soc. of Civil Eng., New York.

Lowe, R. J., J. R. Koseff, and S. G. Monismith (2005a), Oscillatory flow through submerged canopies: 1. Velocity structure, *J. Geophys. Res.*, *110*, C10016, doi:10.1029/2004JC002788.

Lowe, R. J., J. R. Koseff, S. G. Monismith, and J. L. Falter (2005b), Oscillatory flow through submerged canopies: 2. Canopy mass transfer, *J. Geophys. Res.*, *110*, C10017, doi:10.1029/2004JC002789.

Lowe, R. J., J. L. Falter, J. R. Koseff, S. G. Monismith, and M. J. Atkinson (2007), Spectral wave flow attenuation within submerged canopies: Implications for wave energy dissipation, *J. Geophys. Res.*, *112*, C05018, doi:10.1029/2006JC003605.

Luhar, M., J. Rominger, and H. Nepf (2008), Interaction between flow, transport and vegetation spatial structure, *Environ. Fluid Mech.*, *8*, 423–439, doi:10.1007/s10652-008-9080-9.

Madsen, O. (1971), On the generation of long waves, *J. Geophys. Res.*, *76*(36), 8672–8683, doi:10.1029/JC076i036p08672.

Marbà, N., C. M. Duarte, J. Cebrian, M. E. Gallegos, B. Olesen, and K. Sand-Jensen (1996), Growth and population dynamics of *Posidonia oceanica* on the Spanish Mediterranean coast: Elucidating seagrass decline, *Mar. Ecol. Prog. Ser.*, *137*(1–3), 203–213, doi:10.3354/meps137203.

Marin, F. (2004), Eddy viscosity and Eulerian drift over rippled beds in waves, *Coastal Eng.*, *50*, 139–159, doi:10.1016/j.coastaleng.2003.10.001.

Mei, C. C., M. Stiassnie, and D. K.-P. Yue (2005), *Theory and Applications of Ocean Surface Waves*, World Sci., Singapore.

Mendez, F. J., and I. J. Losada (2004), An empirical model to estimate the propagation of random breaking and non-breaking waves over vegetation fields, *Coastal Eng.*, *51*, 103–118, doi:10.1016/j.coastaleng.2003.11.003.

Méndez, F. J., I. J. Losada, and M. A. Losada (1999), Hydrodynamics induced by wind waves in a vegetation field, *J. Geophys. Res.*, *104*(C8), 18,383–18,396, doi:10.1029/1999JC900119.

Nepf, H. M., and E. R. Vivoni (2000), Flow structure in depth-limited, vegetated flow, *J. Geophys. Res.*, *105*(C12), 28,547–28,557, doi:10.1029/2000JC900145.

Pergent-Martini, C., V. Rico-Raimondino, and G. Pergent (1994), Primary production of *Posidonia oceanica* in the Mediterranean Basin, *Mar. Biol. Berlin*, *120*, 9–15.

Peterson, C. H., H. C. Summerson, and P. B. Duncan (1984), The influence of seagrass cover on population structure and individual growth rate of a suspension-feeding bivalve, *Mercenaria mercenaria*, *J. Mar. Res.*, *42*(1), 123–138, doi:10.1357/002224084788506194.

Santos, S. L., and J. L. Simon (1974), Distribution and abundance of the polychaetous annelids in a south Florida estuary, *Bull. Mar. Sci.*, *24*, 669–689.

Sarpkaya, T., and M. Isaacson (1981), *Mechanics of Wave Forces on Offshore Structures*, Van Nostrand Reinhold, New York.

Stoner, A. W. (1980), The role of seagrass biomass in the organization of benthic macrofaunal assemblages, *Bull. Mar. Sci.*, *30*, 537–551.

Temmerman, S., T. J. Bouma, J. Van de Koppel, D. Van der Wal, M. B. De Vries, and P. M. J. Herman (2007), Vegetation causes channel erosion in a tidal landscape, *Geology*, *35*, 631–634, doi:10.1130/G23502A.1.

Terrados, J., P. Ramirez-Garcia, O. Hernandez-Martinez, K. Pedraza, and A. Quiroz (2008), State of *Thalassia testudinum* Banks ex Konig meadows in the Veracruz Reef system, Veracruz, Mexico, *Aquat. Bot.*, *88*(1), 17–26, doi:10.1016/j.aquabot.2007.08.003.

Thomas, F. I. M., and C. D. Cornelisen (2003), Ammonium uptake by seagrass communities: Effects of oscillatory versus unidirectional flow, *Mar. Ecol. Prog. Ser.*, *247*, 51–57, doi:10.3354/meps247051.

Trowbridge, J. H., and O. S. Madsen (1984), Turbulent wave boundary layers, 2, Second-order theory and mass transport, *J. Geophys. Res.*, *89*(C5), 7999–8007, doi:10.1029/JC089iC05p07999.

Vermaat, J. E., N. S. R. Agawin, C. M. Duarte, M. D. Fortes, N. Marbà, and J. S. Uri (1995), Meadow maintenance, growth and productivity of a mixed Philippine seagrass bed, *Mar. Ecol. Prog. Ser.*, *124*(1–3), 215–225, doi:10.3354/meps124215.

Vogel, S. (1994), *Life in Moving Fluids*, Princeton Univ. Press, Princeton, N. J.

Ward, L. G., W. Michael Kemp, and W. R. Boynton (1984), The influence of waves and seagrass communities on suspended particulates in an estuarine embayment, *Mar. Geol.*, *59*(1–4), 85–103, doi:10.1016/0025-3227(84)90089-6.

Zhou, C. Y., and J. M. R. Graham (2000), A numerical study of cylinders in waves and currents, *J. Fluids Structures*, *14*, 403–428, doi:10.1006/jfls.1999.0276.

Zimmerman, R. C. (2003), A bio-optical model of irradiance distribution and photosynthesis in seagrass canopies, *Limnol. Oceanogr.*, *48*, 568–585, doi:10.4319/lo.2003.48.1_part_2.0568.

S. Coutu, Institut d'Ingénieurie de l'Environnement, Ecole Polytechnique Fédérale de Lausanne, GR A1 445, Station 2, CH-1015 Lausanne, Switzerland.

S. Fox, M. Luhar, and H. Nepf, Department of Civil and Environmental Engineering, Massachusetts Institute of Technology, 15 Vassar St., 48-216, Cambridge, MA 02139, USA. (mluhar@mit.edu)

E. Infantes, Instituto Mediterráneo de Estudios Avanzados, IMEDEA (CSIC-UIB), Miquel Marqués 21, 07190 Esporles, Spain.